Optimization of Hoisting Attitude in Non-standard Steel Structures via Adjustable Counterweight Balance Beam Technology

Wenlei Li[1], Zhiping Deng[2*], Xiaoshan Liu[1], Xiaoping Jiang[3]

[1] Department of Structural Engineering Research, Beijing Special Engineering and Design Institute, 100028 Beijing, China

[2] Department of Military Installations, Army Logistics Academy of PLA, 401311 Chongqing, China

[3] Department of Engineering Design, Logistics Support Department of PLA, 100036 Beijing, China

* Correspondence: Zhiping Deng (dzpcorner@163.com)

Abstract: In addressing the challenge of precise lateral attitude adjustment during high-altitude hoisting of non-standard steel structures, such as the rotating platforms in rocket launch towers, a novel approach involving an adjustable counterweight balance beam has been developed. This method entails the strategic placement of movable counterweight blocks on the balance beam, thereby enabling the manipulation of the gravity center's distribution for refined posture control of the load suspended beneath the beam. A theoretical model encompassing static balance and deformation coordination has been formulated for this adjustable balance beam system. Utilizing Matlab for computational analysis, the model elucidates the effects of various parameters, including the counterweight block position, block weight, lifted load, sling length, and balance beam length on the beam's attitude. The findings suggest that the beam's performance can be optimized in accordance with the weight of the load. Through the judicious design of the sling and beam lengths, as well as the counterweight block mass, continuous fine-tuning of the hoisting posture is achievable via progressive adjustments of the counterweight block's position on the balance beam. The theoretical calculations and analyses derived from this study offer valuable insights for the design of new balance beams and the enhancement of hoisting operations, catering to the specific demands of high-precision, high-altitude lifting tasks.

Keywords: Hoisting attitude optimization; Adjustable balance beam; Counterweight technology; Non-standard steel structure; High-altitude precision lifting

1 Introduction

Recent advancements in the capabilities of large lifting machinery, specifically in terms of load capacity, cantilever lifting height, and amplitude, have significantly propelled the development of integral lifting technology [1–5]. This approach, when contrasted with traditional split lifting methods [6–9], has been observed to offer enhanced efficiency, reduced high-altitude work requirements, and greater safety and reliability. Moreover, the quality of ground welding, in the context of these operations, has been noted to exhibit improved efficiency and reliability [10–12]. In integral lifting operations, the design of a balance beam is a critical component to ensure the equilibrium of the suspended element or equipment, prevent potential damage from slings, and distribute the load at the lifting point effectively [13–15]. Typically, the integral hoisting process involves vertical docking between the suspended member or equipment and the ground base [16]. Adjustments in the hoisting posture are commonly facilitated by the implementation of pulleys and wind ropes on the balance beam [17–20]. However, in scenarios involving lateral high-altitude docking, such as in the lifting of non-standard steel structures like rotating platforms of rocket launch towers, the precision required for attitude adjustment in mid-air is notably higher. Traditional methods employing pulleys and wind ropes have been identified as less efficient in these contexts.

To address this technical challenge in high-precision lateral attitude adjustment, the introduction of movable and adjustable counterweight blocks on the balance beam has been proposed. This modification allows for the alteration of the balance beam's center of gravity distribution, thereby enabling fine-tuning of both the beam's balance and

the posture of the load beneath it. Such an innovation promises to enhance the accuracy and efficiency of integral lifting operations. This study presents a theoretical investigation into this novel approach, focusing on identifying the adjustable range of attitude and influencing factors under varied lifting conditions and counterweight configurations. The findings aim to guide the design of new counterweight adjustable balance beams, contributing significantly to the field of high-precision lifting.

2 Theoretical Model

The theoretical model for this study is elucidated with reference to Figure 1, depicting a rectangular balance beam, ABCD, characterized by dimensions L_1 and L_2. To enhance the sensitivity of gravity center adjustments within the balance beam system, counterweight blocks are strategically positioned at the edges of the beam. Tracks, aligned with the perimeter of the beam, facilitate the motor-driven movement of slide blocks along each side. It is assumed that both the balance beam and counterweight blocks are rigid bodies. The slings connecting the balance beam and the load are of equal length and maintain parallelism throughout the lifting process. Consequently, the spatial attitude changes of the load mirror those of the balance beam, permitting the consideration of the load's gravity as acting centrally on the beam. A spatial rectangular coordinate system is established, taking the convergence points of the four slings on the balance beam as the origin, as illustrated in Figure 1.
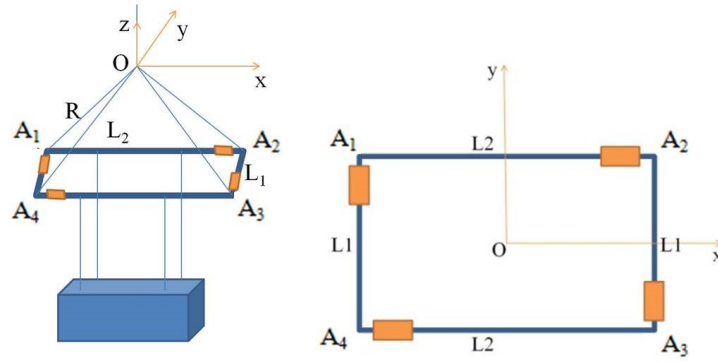
Figure 1. Adjustable balance beam and coordinate system

The lifting points, located at the four corners of the balance beam, are denoted as $A_i\,(x_i, y_i, z_i)$, where i ranges from 1 to 4. The system encompasses 12 degrees of freedom, necessitating the formulation of 12 independent equations for problem-solving. These comprise 7 independent geometric equations and 5 static equilibrium equations.

The geometric equations:

$$\overrightarrow{A_1\,A_4} \cdot \overrightarrow{A_1\,A_2} = (x_4 - x_1)(x_2 - x_1) + (y_4 - y_1)(y_2 - y_1) + (z_4 - z_1)(z_2 - z_1) = 0 \tag{1}$$

$$\overrightarrow{A_2\,A_1} \cdot \overrightarrow{A_2\,A_3} = (x_1 - x_2)(x_3 - x_2) + (y_1 - y_2)(y_3 - y_2) + (z_1 - z_2)(z_3 - z_2) = 0 \tag{2}$$

$$\overrightarrow{A_3\,A_2} \cdot \overrightarrow{A_3\,A_4} = (x_2 - x_3)(x_4 - x_3) + (y_2 - y_3)(y_4 - y_3) + (z_2 - z_3)(z_4 - z_3) = 0 \tag{3}$$

$$\left|\overrightarrow{A_1\,A_2}\right| = \sqrt{(x_2 - x_1)^2 + (y_2 - y_1)^2 + (z_2 - z_1)^2} = L_2 \tag{4}$$

$$\left|\overrightarrow{A_2\,A_3}\right| = \sqrt{(x_3 - x_2)^2 + (y_3 - y_2)^2 + (z_3 - z_2)^2} = L_1 \tag{5}$$

$$\left|\overrightarrow{A_3\,A_4}\right| = \sqrt{(x_4 - x_3)^2 + (y_4 - y_3)^2 + (z_4 - z_3)^2} = L_2 \tag{6}$$

$$y_2 - y_4 = (x_2 - x_4)(L_1/L_2) \tag{7}$$

Referring to the isolated body shown in Figure 2, the static equilibrium equation for the spatial force system is defined:

$$\sum_{i=1}^{4} F_i x_i = 0 \tag{8}$$

12

$$\sum_{i=1}^{4} F_i y_i = 0 \qquad (9)$$

$$\sum_{i=1}^{4} F_i z_i + \sum_{i=1}^{4} G_i + G = 0 \qquad (10)$$

$$\sum_{i=1}^{4} G_i \left(x_i + u_1 \left(x_{i-1} - x_i \right) \right) + G \left(x_2 + x_4 \right)/2 = 0, if \ i = 1, x_{i-1} = x_4 \qquad (11)$$

$$\sum_{i=1}^{4} G_i \left(y_i + u_i \left(y_{i-1} - y_i \right) \right) + G \left(y_2 + y_4 \right)/2 = 0, if \ i = 1, x_{i-1} = x_4 \qquad (12)$$

where, parameters include the length of the sling (R), the elastic modulus of the sling (E), the cross-sectional area of the sling (S), $S = \pi(d/2)^2$, and the diameter of the sling (d). The sliding distances of the slide block along each beam edge, H_1, H_2, H_3 and H_4, and their relative sliding are represented as $u_1 = H_1/L_1$, $u_2 = H_2/L_2$, $u_3 = H_3/L_1$ and $u_4 = H_4/L_2$, respectively. Forces exerted by the slings at lifting points A_1, A_2, A_3 and A_4 are expressed as F_1, F_2, F_3 and F_4, respectively:

$$F_i = ES \frac{\sqrt{x_i^2 + y_i^2 + z_i^2} - R}{R}, i = 1 \sim 4 \qquad (13)$$
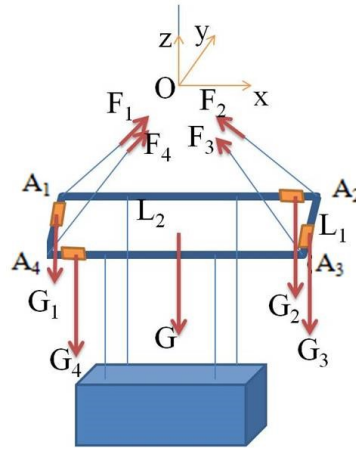
Figure 2. Spatial force system diagram of isolated body

By inputting the sliding distances H_1, H_2, H_3, H_4 the spatial coordinates of A_1, A_2, A_3, A_4 are derived from Eqs. (1) to (12). This enables an analysis of the attitude changes.

3 Solving and Analysis of the Model

For the resolution and analysis of Eqs. (1) to (12), MATLAB programming was employed. The elastic modulus of the sling was set at 210 GPa to facilitate the calculation and analysis of attitude adjustments under varying parameters such as the weight of the counterweight blocks, the mass of the objects being lifted, the length of the sling, and the dimensions of the balance beam.

The initial arrangement of the sliders was symmetrically positioned at the vertices of the balance beam. This configuration placed the initial equivalent center of the four sliders at the midpoint of the balance beam. The spatial orientation of the balance beam is modifiable through the positional adjustments of three of the sliders. In this analysis, it was postulated that the fourth slider remains stationary at its initial location. The study thus focused on the alterations in the balance beam's attitude brought about by varying the positions of the other three sliders. The spatial orientation of the balance beam is quantified by measuring the angle between the plane's normal line and the X, Y, and Z axes. When the sliders are positioned at their initial points, the normal line of the balance beam plane aligns parallel to the Z axis. Changes in orientation are denoted as D-X, D-Y, and D-Z, representing the shifts in degrees between the normal line and the respective X, Y, and Z axes.

3.1 The Influence of the Counterweight Position

The combined mass of the lifting weight and the balance beam was established at 1000 kN. Each counterweight block was assigned a weight of 10 kN. For the slings, a specification of 50 mm in diameter and 5 m in length was chosen. The dimensions of the balance beam were set with a width (L_2) of 3 m and a length (L_1) of 6 m, and the slings were positioned at an approximate angle of 45° relative to the horizontal plane. The study examined the scenario where u_2 and u_3 values were set to zero, focusing on the resultant variations in the angles D-X, D-Y, and D-Z. These angles represent the shifts between the normal of the balance beam plane and the X, Y, and Z axes, respectively, as a function of the variable u_1. These variations and their relationship with u_1 are illustrated in Figure 3.


(a)

(b)

(c)
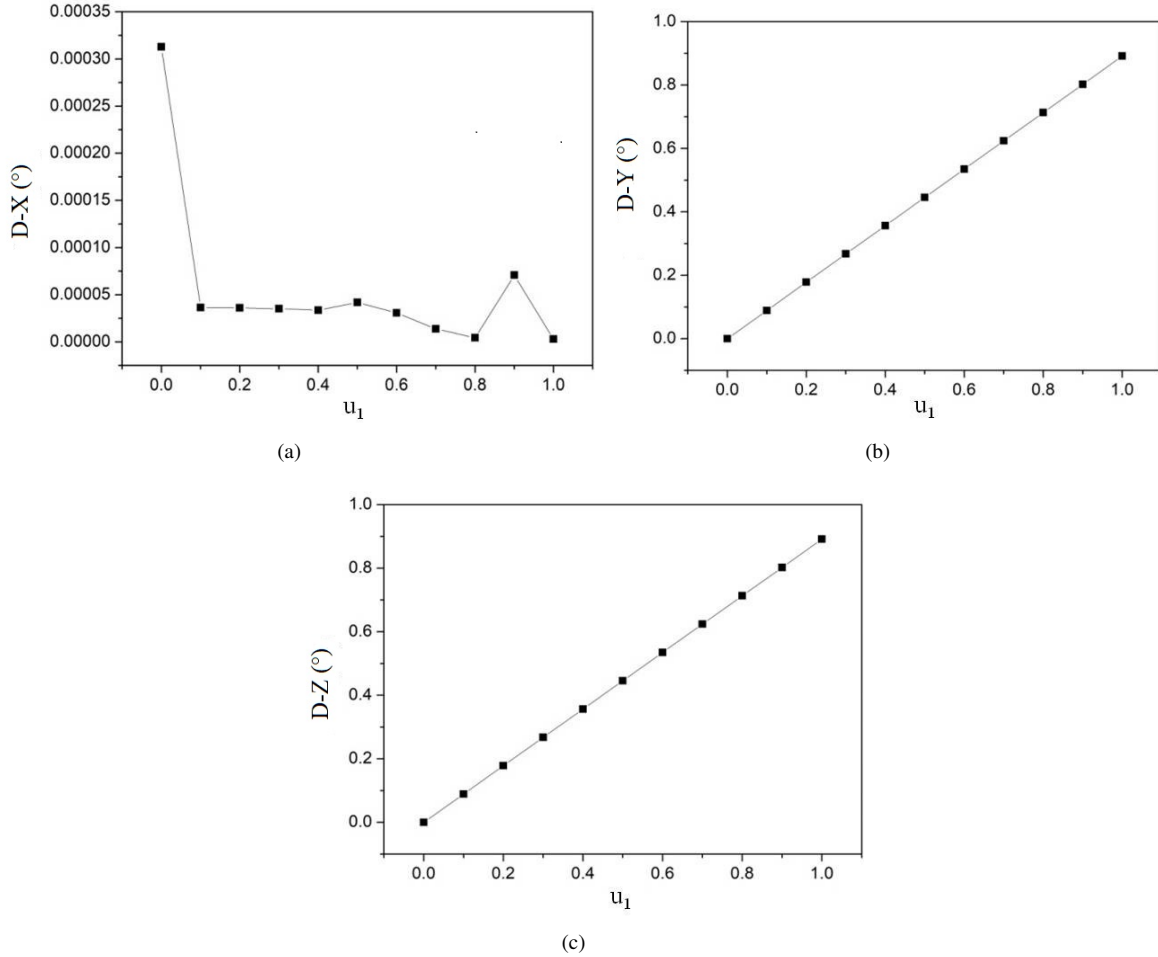
Figure 3. The variation of D-X, D-Y and D-Z with u_1

When $u_1 = u_3 = 0$, the changes of D-X, D-Y and D-Z angles between the normal of the plane of the balance beam and the X, Y and Z axes with u_2 are shown in Figure 4.

Figure 3 demonstrates that with counterweight blocks 2 and 3 remaining static, altering the position of counterweight block 1 influences the angle D-X, defined as the angle between the normal of the balance beam plane and the X-axis. As observed, D-X approaches zero, indicating that the rotation of the balance beam predominantly occurs around the X-axis. Concurrently, the angles between the normal of the balance beam plane and the Y and Z axes exhibit an increase in tandem with u_1's increment. At the point where u_1 equals 1, representing the maximum displacement of counterweight block 1, the largest observed angle between the normal of the balance beam plane and both the Y and Z axes is approximately 0.891°.

Similarly, as depicted in Figure 4, when counterweight blocks 1 and 3 are held constant and only the position of counterweight block 2 is varied, the variable D-X again trends towards zero, indicating a primary rotation of the balance beam around the Y axis. The angles between the normal of the balance beam plane and the X and Z axes also increase as u_2 is incremented. At u_2's maximum value of 1, where counterweight block 2 reaches its furthest extent, the maximum angle between the normal of the balance beam plane and the X and Z axes is recorded at 0.446°.

(a)

(b)

(c)
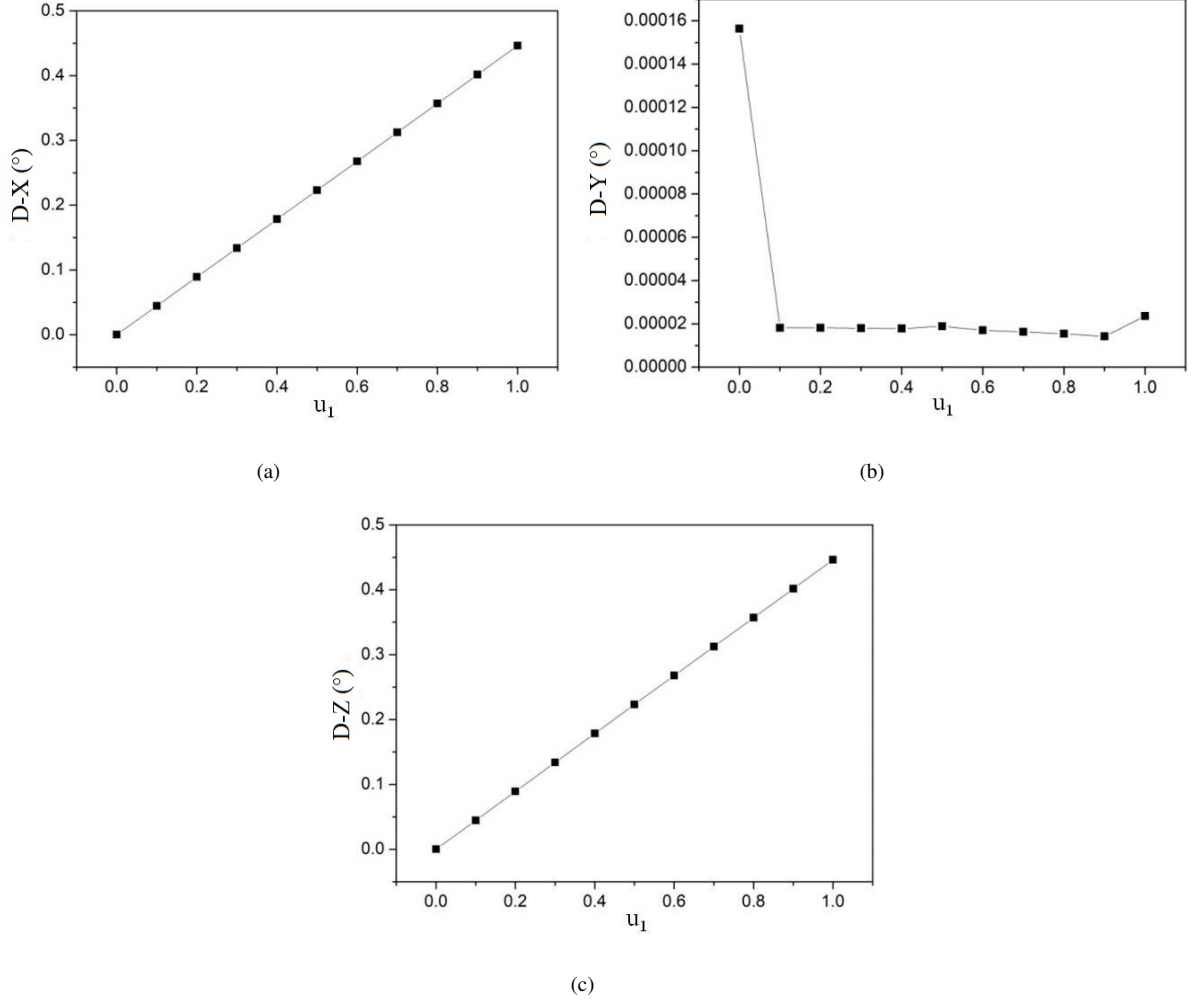
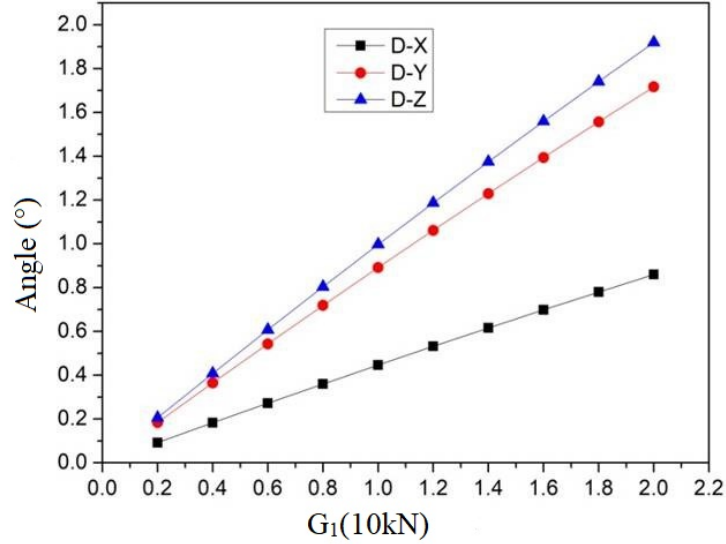**Figure 4.** The variation of D-X, D-Y and D-Z with u_2

Table 1. The maximum value of D-X, D-Y, and D-Z

	Maximum Value (°)	u_1	u_2	u_3
$D-X$	0.446	0.9	1	1
$D-Y$	0.891	1	0.2	0.2
$D-Z$	0.996	1	1	1

Concurrently, the positions of counterweight blocks 1, 2, and 3 on the balance beam are adjusted, with the peak values of D-X, D-Y, and D-Z outlined in Table 1. This table enumerates the slider positions corresponding to these maximal values. Specifically, a D-X maximum of 0.446° occurs when u_1 equals 0.9 and both u_2 and u_3 are set to 1. Similarly, the highest D-Y value of 0.891° is observed with u_1 at 1 and u_2 and u_3 at 0.2. For D-Z, its zenith of 0.996° is reached when u_1, u_2 and u_3 are all equal to 1.

### 3.2 The Influence of the Weight of Counterweight Block

For this experiment, the combined mass of the lifting load and the balance beam is fixed at 1000kN. A sling with a diameter of 50mm and a length of 5m is employed. The dimensions of the balance beam are set at 3m for width (L_2) and 6m for length (L_1), with the sling forming an approximate 45° angle with the horizontal plane. Altering the weight of the counterweight blocks influences the maximum angle adjustments of D-X, D-Y, and D-Z, as depicted in Figure 5. This figure elucidates a linear correlation between the increased mass of the counterweight blocks and the enhanced angular adjustments, under identical lifting conditions.

Figure 5. The variation of maximum values of D-X, D-Y, and D-Z with the weight G_1

3.3 The Influence of the Weight to be Lifted

Each slider is assigned a weight of 10kN, and a sling featuring a 50mm diameter and 5m length is selected. The balance beam dimensions are specified, with a width (L_2) of 3m and a length (L_1) of 6m. The sling is oriented at approximately a 45° angle relative to the horizontal plane. In scenarios varying both the lifting weights and the total mass of the balance beam, the positions of sliders 1, 2, and 3 are simultaneously adjusted. Correspondingly, the maximal alterations in the angles D-X, D-Y, and D-Z – which signify the angle deviation between the balance beam's normal plane and the X, Y, and Z axes – are observed to vary with the combined weight of the lifting loads and the balance beam. This variation is graphically represented in Figure 6.
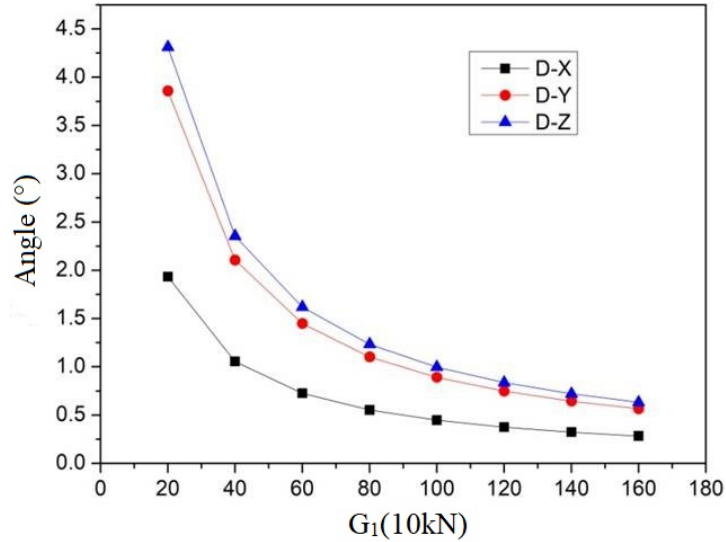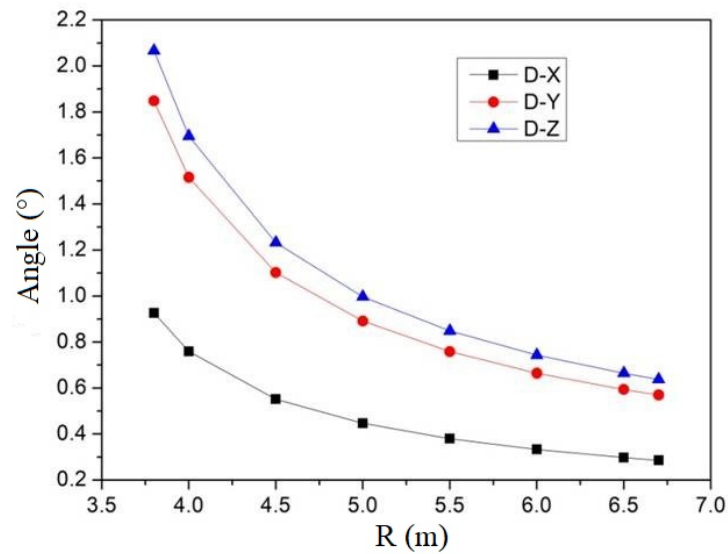

Figure 6. The variation of maximum values of D-X, D-Y, and D-Z with the weight G

Figure 6 elucidates that, under consistent conditions for the counterweight block weight and other factors, there is a noticeable trend in the balance beam's attitude adjustment capabilities. Specifically, as the weight of the load increases, the maximum achievable attitude adjustment of the balance beam diminishes, illustrating a nonlinear relationship. Additionally, an observable trend line, approaching parallelism with the coordinate axis's horizontal axis, emerges. This trend indicates that beyond a certain threshold in the weight of the load, adjustments in the position of the counterweight block yield negligible alterations in the balance beam's attitude.

3.4 The Influence of Length of the Sling

In this configuration, each slider possesses a mass of 10 kN, while the combined weight of the load and the balance beam totals 1000 kN. A sling with a 50mm diameter is utilized, alongside a balance beam measuring 3m in width and 6m in length. Investigating the impact of varying sling lengths, adjustments are concurrently made to the positions of sliders 1, 2, and 3. This procedure facilitates the examination of the maximal alterations in D-X, D-Y, and D-Z — these being the angles between the normal to the balance beam plane and the X, Y, and Z axes, respectively. As depicted in Figure 7, the sling length under consideration ranges from 3.8m to 6.7m. This range corresponds to a change in the angle between the sling and the horizontal plane from 30° to 60°.

Figure 7 illustrates that, under constant conditions such as the weight of the counterweights and the load to be lifted, the maximum amplitude for adjusting the balance beam's orientation demonstrates a nonlinear decrease with an increase in the sling's length. Specifically, this indicates that a smaller angle between the sling and the horizontal plane allows for a more extensive range in adjusting the balance beam's attitude.

Figure 7. The variation of maximum values of D-X, D-Y, and D-Z with the sling length R

3.5 The Influence of Length of the Balance Beam
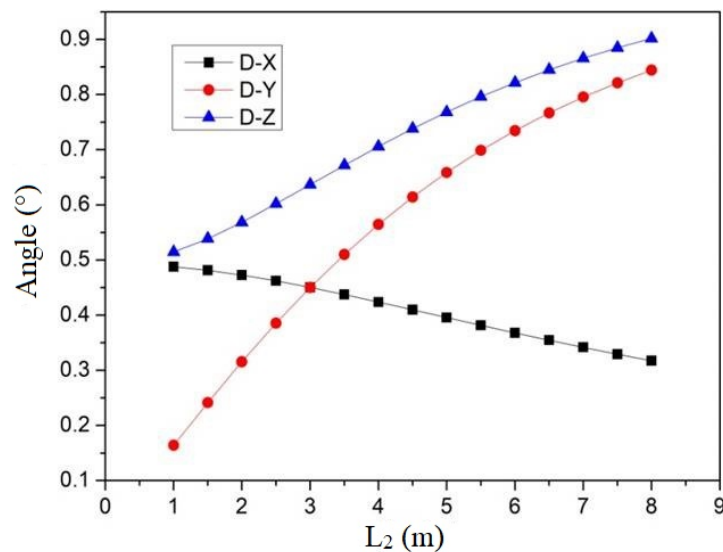
**Figure 8.** The variation of maximum values of D-X, D-Y, and D-Z with the length L_2

With each slider weighing 10kN and the combined weight of the load and balance beam totaling 1000kN, a 50mm diameter sling was selected. The width of the balance beam, L_2, was set at 3 meters. Maintaining a consistent

45° angle between the sling and the horizontal plane, the positions of sliders 1, 2, and 3 were simultaneously adjusted corresponding to various lengths of the balance beam, L_1. Figure 8 depicts the resultant maximum variations in the angles D-X, D-Y, and D-Z, which represent the angular deviations between the normal of the balance beam plane and the X, Y, and Z axes, respectively. These variations are presented in relation to the changing length of the balance beam.

Figure 8 illustrates that under consistent conditions—such as the weight of the counterweight block, the load weight, the width of the balance beam, and the angle between the sling and the horizontal plane—the maximum D-Z value, representing the angle between the balance beam's plane normal and the Z-axis, increases as the length of the balance beam (L_2) extends. This observation indicates that the maximum variation in the D-Z angle predominantly depends on the circumference of the balance beam. Conversely, the maximum value of the D-X angle, indicating the deviation between the plane normal of the balance beam and the X-axis, diminishes with an increase in L_2. In contrast, the maximum value of the D-Y angle—reflecting the angular variation between the balance beam's plane normal and the Y-axis—rises with L_2's elongation. Notably, when L_2 equals L_1 at 3 meters, these two angles are equivalent. This suggests that the ratio of the balance beam's length to its width significantly influences the distribution of angular changes between the plane normal of the balance beam and the X and Y axes.

4 Design Procedure
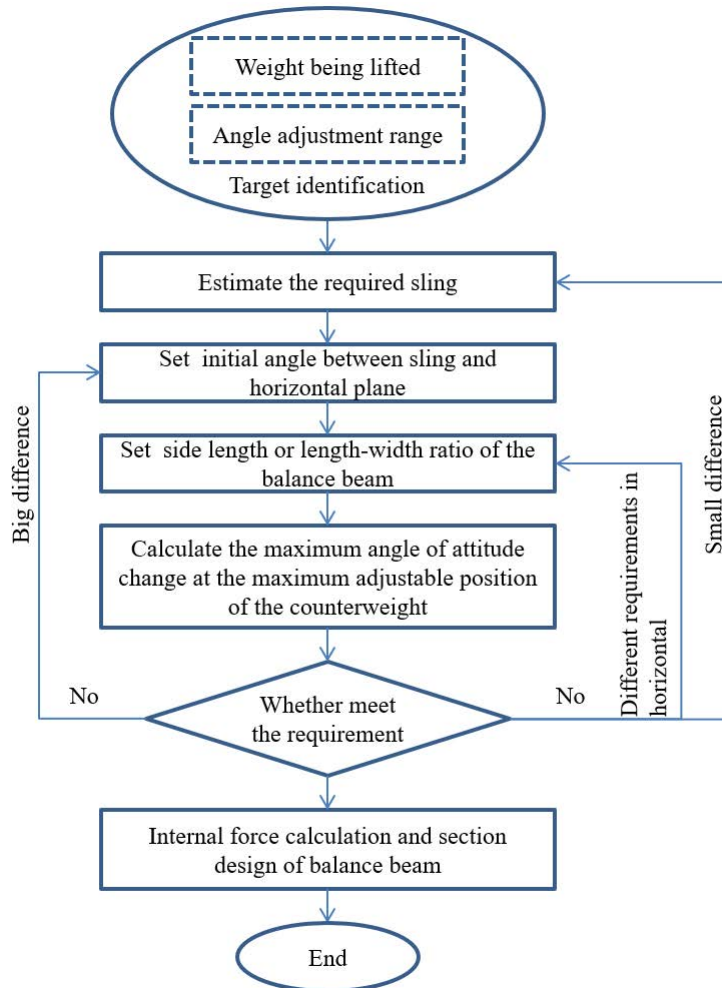
Figure 9. Design flowchart of the counterweight adjustable balance beam

The computational and analytical findings laid out earlier lead to the formulation of design procedures for the counterweight adjustable balance beam, as depicted in Figure 9. The process begins with determining the weight of the object to be lifted and the required range of its hoisting attitude angle adjustment. Based on the weight of the object, an initial estimate of the sling's thickness and the material's elastic modulus is made, presuming an angle of approximately 45° between the sling and the horizontal plane. It is initially assumed that the balance beam is square, setting a preliminary value for its side length. Utilizing the model outlined in this paper, the maximum change in

attitude angle at the counterweight's limit of adjustability is calculated. This result is then compared with the required angle adjustment range. Should there be a significant discrepancy, the side length and the angle between the sling and the horizontal plane are adjusted and recalculated. If the adjustment amplitude in the horizontal direction is off, the square balance beam design is modified into a rectangular shape, and the aspect ratio is tweaked for further trial calculations. The final step involves conducting internal force calculations and the sectional design of the balance beam.

5 Conclusion

(1) It has been demonstrated that through the judicious design of sling length, balance beam length, and counterweight block weight, the continuous adjustment of the counterweight block position on the balance beam facilitates the fine-tuning of hoisting posture in a continuous manner.

(2) The investigation has revealed that when altering the position of a single counterweight block, the spatial attitude change of the balance beam is approximately proportional to the displacement of said counterweight block.

(3) Observations indicate that, under constant conditions including counterweight block weight, the balance beam's maximum attitude adjustment capability diminishes as the weight of the lifted object increases, following a nonlinear relationship.

(4) Analyses suggest that, with other variables held constant, the maximum alteration in the angle (D-Z) between the normal of the balance beam plane and the Z-axis escalates with the elongation of balance beam length L_2.

(5) Similarly, it has been ascertained that, maintaining constant conditions, the maximum variation in the angle (D-X) between the normal of the balance beam plane and the X-axis reduces with the increment of balance beam length L_2, whereas the maximum alteration in the angle (D-Y) between the normal of the plane and the Y-axis heightens as balance beam length L_2 increases.

Data Availability

The data used to support the findings of this study are available from the corresponding author upon request.

Conflicts of Interest

The authors declare that they have no conflicts of interest.

References

[1] L. Tian, J. Hao, J. Wei, and J. Zheng, "Integral lifting simulation of long-span spatial steel structures during construction," *Autom. Constr.*, vol. 70, pp. 156–166, 2016. https://doi.org/10.1016/j.autcon.2016.06.015

[2] M. Zhu, X. Chen, and Z. Guo, "Construction analysis on integral lifting of steel structure by the vector form intrinsic finite element," *J. Southeast Univ. (English Edition)*, vol. 32, no. 4, pp. 451–456, 2016.

[3] T. Kim, H. Lim, H. Cho, and K. Kang, "Automated lifting system integrated with construction hoists for table formwork in tall buildings," *J. Constr. Eng. Manag.*, vol. 140, no. 10, p. 04014049, 2014. https://doi.org/10.1061/(ASCE)CO.1943-7862.0000884

[4] A. J. Haywood and B. H. Schaub, "The integration of lifting foils into ride control systems for fast ferries," *Aust. J. Mech. Eng.*, vol. 3, no. 2, pp. 133–141, 2006. https://doi.org/10.1080/14484846.2006.11464502

[5] S. Yao, W. Zhao, and Q. Cheng, "Aerial steel platform overall lifting process and stress calculation," *Appl. Mech. Mater.*, vol. 681, pp. 222–228, 2014. https://doi.org/10.4028/www.scientific.net/AMM.681.222

[6] Z. Krimi, Z. Lafhaj, and L. Ducoulombier, "Prospective study on the integration of additive manufacturing to building industry—case of a French construction company," *Addit. Manuf.*, vol. 16, pp. 107–114, 2017. https://doi.org/10.1016/j.addma.2017.04.002

[7] M. A. B. A. Majid, M. S. B. M. Nor, and H. B. M. Hanafi, "Case study-hull block heavy lifting challenges for a tension leg platform TLP," in *Offshore Technology Conference Asia*, 2016, p. D021S017R004. https://doi.org/10.4043/26729-MS

[8] A. D. Monte, M. C. Raciti, and E. Benini, "A retrospective of high-lift device technology," *Int. J. Aerosp. Mech. Eng.*, vol. 6, no. 11, pp. 2561–2566, 2012.

[9] M.-D. Lee, M.-K. Won, U.-K. Lee, H.-H. Cho, and K.-I. Kang, "Integrated lifting model of planning and operation for finishing works in tall building construction," *J. Archit. Inst. Korea Struct. Constr.*, vol. 30, no. 5, pp. 125–133, 2014. https://doi.org/10.5659/JAIK_SC.2014.30.5.125

[10] Y. Zhao, J. Wang, and M. Pang, "Integral lifting project of the qifeng bridge," *J. Perform. Constr. Facil.*, vol. 26, no. 3, pp. 353–361, 2012. https://doi.org/10.1061/(ASCE)CF.1943-5509.0000211

[11] M. J. Skibniewski and L. C. Chao, "Evaluation of advanced construction technology with AHP method," *J. Constr. Eng. Manag.*, vol. 118, no. 3, pp. 577–593, 1992. https://doi.org/10.1061/(ASCE)0733-9364(1992)118:3(577)

[12] G. N. Teixeira and D. J. Schiozer, "Integration of production facilities and reservoir simulation for comparison of subsea and conventional lift technologies," in *EAGE Annual Conf. & Exhib. incorp. SPE Europec*, 2013. https://doi.org/10.2118/164850-MS

[13] M. Shen, H. Chang, W. Zhang, Q. Li, and C. Wen, "Anti-deformation design of thin-wall large-span box structure during lifting by layers," *At. Energ. Sci. Technol.*, vol. 56, pp. 189–199, 2022. https://doi.org/10.7538/yzk.2022.youxian.0113

[14] M. Yu, X. Yao, N. Deng, T. Hao, L. Wang, and H. Wang, "Optimal cable force adjustment for long-span concrete-filled steel tube arch bridges: Real-time correction and reliable results," *Buildings*, vol. 13, no. 9, p. 2214, 2023. https://doi.org/10.3390/buildings13092214

[15] C. Sydora, Z. Lei, M. F. F. Siu, S. Han, and U. Hermann, "Critical lifting simulation of heavy industrial construction in gaming environment," *Facilities*, vol. 39, no. 1/2, pp. 113–131, 2021. https://doi.org/10.1108/F-08-2019-0088

[16] S. J. Bianco, C. T. Chevalier, J. S. Litt, J. K. Smith, J. W. Chapman, and J. L. Kratz, "Revolutionary vertical lift technology (RVLT) side-by-side hybrid concept vehicle powertrain dynamic model," in *Amer. Soc. Mech. Eng.*, 2021. https://doi.org/10.1115/GT2021-59375

[17] Y. Zhang, X. Tang, D. Chen, and B. Ji, "Posture adjustment and control algorithm for integral synchronous lifting of bridge," *Adv. Mater. Res.*, vol. 163-167, pp. 2625–2631, 2011. https://doi.org/10.4028/www.scientific.net/AMR.163-167.2625

[18] B. Dai, K. Lei, S. Yu, B. Jia, X. Zhang, J. Yan, and X. Chen, "The construction process simulation and in-situ monitoring of Nanjing Niushou mountain dendritic structure," *Proc. IASS Annu. Symp.*, vol. 2018, no. 4, pp. 1–8, 2018.

[19] R. Chudley and R. Greeno, *Construction Technology*. Pearson Education, 2005.

[20] W. Zhang, S. Yu, X. Zhang, J. Yan, and X. Chen, "Construction process simulation and in situ monitoring of dendritic structure on Nanjing Niushou mountain," *Shock Vib.*, vol. 2019, 2019. https://doi.org/10.1155/2019/1873479

Appendix

Matlab calculation program

```
u = [];
u(1) = 0;
u(2) = 0;
u(3) = 0;
u(4) = 0;
u(5) = 5;
u(6) = 5;
u(7) = 7;
u(8) = 10;
u(9) = 1000;
u(10) = 210;
u(11) = 3.14 * (50/2)^2;
1 = u(5);
L2 = u(6);
R = u(7);
G1 = u(8);
G = u(9);
E = u(10);
A = u(11);
zzz = sqrt(R^2 - (sqrt(L1^2 + L2^2)/2)^2);
x0(1) = -L2/2;
x0(2) = L1/2;
x0(3) = -zzz;
x0(4) = L2/2;
x0(5) = L1/2;
x0(6) = -zzz;
x0(7) = L2/2;
x0(8) = -L1/2;
x0(9) = -zzz;
```

```matlab
x0(10) = -L2/2;
x0(11) = -L1/2;
x0(12) = -zzz;
rot = [];
loc = [];
cont = 1;
for i = 0 : 0.2 : 1
    for j = 0 : 0.2 : 1
        for k = 0 : 0.2 : 1
            u(1) = i;
            u(2) = j;
            u(3) = k;    xx = fsolve(@(x)lifting(x, u), x0, optimset('MaxFunEvals', 100000,' MaxIter', 1000));
x1 = xx(10) - xx(1); y1 = xx(11) - xx(2); z1 = xx(12) - xx(3);
x2 = xx(4) - xx(1); y2 = xx(5) - xx(2); z2 = xx(6) - xx(3);
            x_f a = y1 * z2 - y2 * z1;
            y_f a = z1 * x2 - z2 * x1;
            z_f a = x1 * y2 - x2 * y1;
            m_f a = sqrt(x_f a^2 + y_f a^2 + z_f a^2);
            rot_x = 90 - acos(abs(x_f a/m_f a)) * 180/pi;
            rot_y = 90 - acos(abs(y_f a/m_f a)) * 180/pi;
            rot_z = acos(abs(z_f a/m_f a)) * 180/pi;
            rot(cont, :) = [rot_x, rot_y, rot_z];
            loc(cont, :) = [i, j, j];
            cont = cont + 1;
        end
    end
end
[M1, I1] = max(rot(:, 1));
[M2, I2] = max(rot(:, 2));
[M3, I3] = max(rot(:, 3));
rot_m ax(1, :) = [rot(I1, 1), loc(I1, 1), loc(I1, 2), loc(I1, 3)];
rot_m ax(2, :) = [rot(I2, 2), loc(I2, 1), loc(I2, 2), loc(I2, 3)];
rot_m ax(3, :) = [rot(I3, 3), loc(I3, 1), loc(I3, 2), loc(I3, 3)];


function S = lifting(x, u)
L1 = u(5);
L2 = u(6);
R = u(7);
G1 = u(8);
G = u(9);
E = u(10);
A = u(11);
S(1) = (x(10) - x(1)) * (x(4) - x(1)) + (x(11) - x(2)) * (x(5) - x(2)) + (x(12) - x(3)) * (x(6) - x(3));
S(2) = (x(1) - x(4)) * (x(7) - x(4)) + (x(2) - x(5)) * (x(8) - x(5)) + (x(3) - x(6)) * (x(9) - x(6));
S(3) = (x(4) - x(7)) * (x(10) - x(7)) + (x(5) - x(8)) * (x(11) - x(8)) + (x(6) - x(9)) * (x(12) - x(9));
S(4) = sqrt((x(4) - x(1))^2 + (x(5) - x(2))^2 + (x(6) - x(3))^2) - L2;
S(5) = sqrt((x(10) - x(7))^2 + (x(11) - x(8))^2 + (x(12) - x(9))^2) - L2;
S(6) = sqrt((x(7) - x(4))^2 + (x(8) - x(5))^2 + (x(9) - x(6))^2) - L1;
S(7) = x(5) - x(11) - (x(4) - x(10)) * (L1/L2);
S(8) = -(E * A * (sqrt(x(1)^2 + x(2)^2 + x(3)^2) - R)/R) * x(3) - (E * A * (sqrt(x(4)^2 + x(5)^2 + x(6)^2) - R)/R) * x(6) - (E * A * (sqrt(x(7)^2 + x(8)^2 + x(9)^2) - R)/R) * x(9) - (E * A * (sqrt(x(10)^2 + x(11)^2 + x(12)^2) - R)/R) * x(12) - 4 * G1 - G;
S(9) = (E * A * (sqrt(x(1)^2 + x(2)^2 + x(3)^2) - R)/R) * x(2) + (E * A * (sqrt(x(4)^2 + x(5)^2 + x(6)^2) - R)/R) * x(5) + (E * A * (sqrt(x(7)^2 + x(8)^2 + x(9)^2) - R)/R) * x(8) + (E * A * (sqrt(x(10)^2 + x(11)^2 + x(12)^2) - R)/R) * x(11);
S(10) = (E * A * (sqrt(x(1)^2 + x(2)^2 + x(3)^2) - R)/R) * x(1) + (E * A * (sqrt(x(4)^2 + x(5)^2 + x(6)^2) - R)/R) * x(4) + (E * A * (sqrt(x(7)^2 + x(8)^2 + x(9)^2) - R)/R) * x(7) + (E * A * (sqrt(x(10)^2 + x(11)^2 + x(12)^2) - R)/R) * x(10);
```

$S(11) = G1 * (x(2) + u(1) * (x(11) - x(2))) + G1 * (x(5) + u(2) * (x(2) - x(5))) + G1 * (x(8) + u(3) * (x(5) - x(8))) + G1 * (x(11) + u(4) * (x(8) - x(11))) + G * ((x(2) + x(8))/2);$

$S(12) = G1 * (x(1) + u(1) * (x(10) - x(1))) + G1 * (x(4) + u(2) * (x(1) - x(4))) + G1 * (x(7) + u(3) * (x(4) - x(7))) + G1 * (x(10) + u(4) * (x(7) - x(10))) + G * ((x(1) + x(7))/2);$